

Polarization-Assisted Transverse and Axial Optical Superresolution

Andrew I. Whiting, Ayman F. Abouraddy, Bahaa E. A. Saleh, Malvin C. Teich

*Quantum Imaging Laboratory, Department of Electrical & Computer Engineering,
Boston University, Boston, MA 02215*

besaleh@bu.edu

John T. Fourkas

Eugene F. Merkert Chemistry Center, Boston College, Chestnut Hill, MA 02467

Abstract: The superposition of two coaxial Gaussian beams with offset foci and orthogonal linear polarizations can be used to produce a right- or left-circular polarization component with a focal spot of volume smaller than that of the Gaussian beam. This polarization-assisted axial and transverse superresolution effect is attributed to the differential Gouy phase shift within the focal region or to the non-Gaussian annular distribution of the circularly-polarized components in the far field.

© 2003 Optical Society of America

OCIS codes: (100.6640) Superresolution; (180.6900) Three-dimensional microscopy

References and links

1. T. R. M. Sales, "Smallest focal spot" *Phys. Rev. Lett.* **81**, 3844-3847 (1998).
2. W. Lukosz, "Optical systems with resolving powers exceeding the classical limit I" *J. Opt. Soc. Am.* **56**, 1463-1472 (1966).
3. W. Lukosz, "Optical systems with resolving powers exceeding the classical limit II" *J. Opt. Soc. Am.* **57**, 932-941 (1967).
4. D. Mendlovic, I. Kiryuschev, Z. Zalevsky, A. W. Lohmann, and D. Farkas, "Two-dimensional superresolution optical system for temporally restricted objects" *Appl. Optics* **36**, 6687-6691 (1997).
5. D. Mendlovic, D. Farkas, Z. Zalevsky, and A. W. Lohmann, "High-frequency enhancement by an optical system for superresolution of temporally restricted objects" *Opt. Lett.* **23**, 801-803 (1998).
6. A. I. Kartashev, "Optical systems with enhanced resolving power" *Opt. Spectrosc. (USSR)* **9**, 204-206 (1960).
7. W. Gartner and A. W. Lohmann, "An experiment going beyond Abbe's limit of Diffraction" *Z. Phys.* **174**, 18-21 (1963).
8. D. Mendlovic and A. W. Lohmann, "Space-bandwidth product adaptation and its application to superresolution: Fundamentals" *J. Opt. Soc. Am. A* **14**, 558-562 (1997).
9. D. Mendlovic, A. W. Lohmann, and Z. Zalevsky, "Space-bandwidth product adaptation and its application to superresolution: Examples" *J. Opt. Soc. Am. A* **14**, 563-567 (1997).
10. Z. Zalevsky, D. Mendlovic, and A. W. Lohmann, "Understanding superresolution in Wigner space" *J. Opt. Soc. Am. A* **17**, 2422-2430 (2000).
11. W. Denk, J. H. Strickler, and W. Webb, "Two-photon laser scanning fluorescence microscopy" *Science* **248**, 73-76 (1990).
12. S. Kawata, H. B. Sun, T. Tanaka, and K. Takada, "Finer features for functional microdevices" *Nature* **412**, 697-698 (2001).
13. S. W. Hell and J. Wichmann, "Breaking the diffraction resolution limit by stimulated emission: stimulated-emission-depletion fluorescence microscopy" *Opt. Lett.* **19**, 780-782 (1994).
14. M. Dyba and S. W. Hell, "Focal spots of size $\lambda/23$ open up far-field fluorescence microscopy at 33 nm axial resolution" *Phys. Rev. Lett.* **88**, 163901 (2002).
15. T. Brixner and G. Gerber "Femtosecond polarization pulse shaping" *Opt. Lett.* **26**, 557-559 (2001).
16. B. E. A. Saleh and M. C. Teich, *Fundamentals of Photonics* (Wiley, New York, 1991).
17. M. Gouy, "Sur la propagation anormale des ondes," *Comp. Rend. Acad. Sci.* **111**, 33-40 (1890).
18. S. Feng and H. Winful, "Physical origin of the Gouy phase shift" *Opt. Lett.* **26**, 485-487 (2001).
19. J. J. Stamnes, *Waves in focal regions* (Adam Hilger, Bristol and Boston, 1986).

20. C. J. Sheppard and Z. S. Hegesdus, "Axial behavior of pupil-plane filters" *J. Opt. Soc. Am. A* **5**, 643-647 (1988).
 21. M. Martinez-Corral, P. Andres, J. Ojeda-Castaneda, and G. Saavedra, "Tunable axial superresolution by annular binary filters - application to confocal microscopy" *Opt. Commun.* **119**, 491-498 (1995).
 22. T. R. M. Sales and G. M. Morris, "Axial superresolution with phase-only pupil filters" *Opt. Commun.* **156**, 227-230 (1998).
 23. Y. Li, "Focal shift and focal switch in dual-focus systems" *J. Opt. Soc. Am. A* **14**, 1297-1304 (1997).
 24. B. Bailey, D. Farkas, D. Taylor, and F. Lanni, "Enhancement of axial resolution in fluorescence microscopy by standing-wave excitation," *Nature* **366**, 44-48 (1993).
 25. M. Born and E. Wolf, *Principles of Optics* (Cambridge University Press, UK, 7th edition, 1999).
-

1. Introduction

Optical microscopy and microlithography play major roles in modern science and technology, and 3D applications have become increasingly important in recent years. Since transverse and axial resolutions limit the size of the 3D objects that may be visualized or fabricated by such systems, the enhancement of resolution beyond the conventional limits is likely to have a great impact on a wide variety of applications. Conventional limits of resolution are set by diffraction, which is governed by the aperture size and shape for both gazing and scanning microscopy and lithography, including confocal systems.

Physical approaches for achieving superresolution, within the domain of classical optics, have been implemented via three major paradigms. In the first of these, the spatial distributions of amplitude and phase apertures within the optical system are modified to reduce the volume of the focal spot [1]. Also within the confines of linear optics, the second approach is based on modifying the characteristics of the optical system, taking account of prior information about the insensitivity of the object to a particular degree of freedom of the optical field. If it is known that the object is stationary, for example, a time-varying optical system (e.g., one that makes use of scanning) can be employed [2, 3, 4, 5]. The same notion can be applied to other degrees of freedom, such as wavelength [6] and polarization [7]. Recent studies on the fractional Fourier transform and optical Wigner distributions have led to a reformulation of superresolution and to new approaches to the subject [8, 9, 10]. In the third approach, a physical characteristic of the object, such as its nonlinear response, is used to supersede the Rayleigh limit. This approach has been used, for example, in multiphoton microscopy [11] and lithography [12], where pairs of photons in the two-photon case, e.g., are absorbed only in a sub-region of the focused illumination beam where the intensity is sufficiently large. A more recent example in which nonlinearity is used for enhancing resolution makes use of stimulated emission to deplete the excitation in a pre-specified region of a pumped medium [13, 14].

In almost all previous resolution enhancement efforts, a scalar wave theory has been adopted and polarization effects have been ignored (although polarization-assisted shaping of the temporal profile of femtosecond pulses has been recently reported [15]). In effect, diffraction and polarization phenomena have been decoupled, while optimal wavefronts and aperture shapes have been pursued. Since changes in the curvature of wavefronts are invariably accompanied by spatially varying phase shifts, the polarization state of an incoming wave is also modified, and this effect is particularly acute upon passage through a focal region. In this paper, we demonstrate how this phenomenon can be harnessed to make a selected polarization component acquire greater confinement in the transverse and axial directions, a technique that we will denote polarization-assisted superresolution (PAS).

2. Polarization and spatial distribution of superposed orthogonally polarized Gaussian beams

To understand the means by which polarization-assisted superresolution can be achieved, consider first the superposition of two coaxial paraxial optical beams in orthogonal polarization states, propagating in a linear, isotropic, and lossless medium. If the beams are of identical

spatial distributions, then the state of polarization of the combined beam will be constant everywhere in space. However, if the beams have different spatial distributions, then the state of polarization of the combined beam will be position dependent since the two beams will be mixed with different weights and phases at different positions. Also, if another polarization component is extracted from the combined beam by use of a polarization-selective device, then it will generally have a spatial distribution different from that of either of the original beams.

To be specific, let the beams be monochromatic Gaussian beams linearly polarized in the x and y directions, and propagating in the z direction. The beams are described by the scalar functions $f_x(\rho, z)$ and $f_y(\rho, z)$, which have different parameters (width or divergence angle, or location of beam center). Here, $\rho = \sqrt{x^2 + y^2}$ is the radial distance. The beams are assumed to have the same frequency so that the complex envelope of the combined beam is the vector sum

$$\mathbf{U}(\rho, z) = f_x(\rho, z)\hat{\mathbf{x}} + f_y(\rho, z)\hat{\mathbf{y}}, \quad (1)$$

where $\hat{\mathbf{x}}$ and $\hat{\mathbf{y}}$ are the appropriate Jones vectors. Clearly, the state of polarization is position dependent since the components of the Jones vector, $f_x(\rho, z)$ and $f_y(\rho, z)$, are position dependent.

In terms of a different orthogonal polarization basis, say right- and left-circular polarization (RCP and LCP), the same complex envelope is written in the form

$$\mathbf{U}(\rho, z) = f_R(\rho, z)\hat{\mathbf{R}} + f_L(\rho, z)\hat{\mathbf{L}}, \quad (2)$$

where

$$f_{R,L}(\rho, z) = \frac{1}{\sqrt{2}}[f_x(\rho, z) \mp j f_y(\rho, z)] \quad (3)$$

are the spatial distributions of the RCP and LCP components, respectively, and $\hat{\mathbf{R}}$ and $\hat{\mathbf{L}}$ are the appropriate Jones vectors. The components $f_R(\rho, z)$ and $f_L(\rho, z)$ are not necessarily Gaussian. This may be readily seen by examining expressions for the intensities of these components,

$$I_{R,L}(\rho, z) = \frac{1}{2}[I_x(\rho, z) + I_y(\rho, z)] \mp [I_x(\rho, z)I_y(\rho, z)]^{1/2} \sin[\phi_x(\rho, z) - \phi_y(\rho, z)], \quad (4)$$

where $I_{x,y}$ and $\phi_{x,y}$ are the intensity and phase associated with $f_{x,y}$.

For simplicity, consider the special case when the x - and y -polarized Gaussian beams have identical parameters but their centers are offset by a distance 2Δ , as illustrated in Fig. 1(a). In this case,

$$I_x(\rho, z) = I(\rho, z - \Delta), \quad I_y(\rho, z) = I(\rho, z + \Delta), \quad (5)$$

$$\phi_x(\rho, z) = \phi(\rho, z - \Delta), \quad \phi_y(\rho, z) = \phi(\rho, z + \Delta) + \xi, \quad (6)$$

where ξ is an additional phase factor introduced into the y component, and $f(\rho, z) = I^{1/2}(\rho, z) \exp[j\phi(\rho, z)]$ represents a Gaussian beam [16],

$$I(\rho, z) = [W_o/W(z)]^2 \exp[-2\rho^2/W^2(z)], \quad \phi(\rho, z) = -kz - k\rho^2/2R(z) + \eta(z). \quad (7)$$

Here, $W(z) = W_o[1 + (z/z_o)^2]^{1/2}$ is the beam width, $R(z) = z[1 + (z_o/z)^2]$ is its radius of curvature, $\eta(z) = \arctan(z/z_o)$ is a phase factor, $W_o = (\lambda z_o/\pi)^{1/2}$ is the beam waist, $2z_o$ is the Rayleigh range, $k = 2\pi/\lambda$, and λ is the wavelength. We have assumed that the beam intensity at its center $(\rho, z) = (0, 0)$ is unity. We will now examine the polarization state of this vector beam, demonstrating that polarization conversion may occur, and determine the spatial distributions of the circularly polarized components, showing that they may exhibit transverse and axial superresolution.

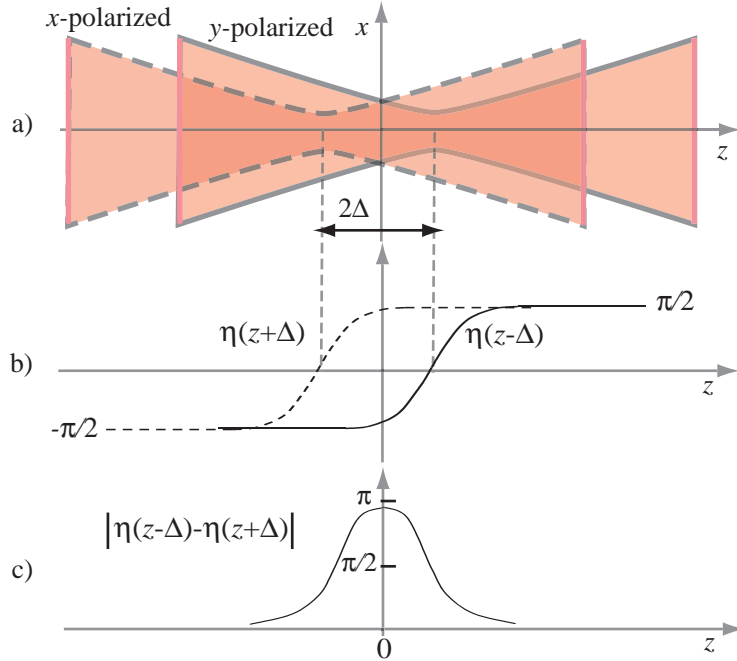


Fig. 1. (a) Superposition of x- and y-polarized coaxial Gaussian beams with centers offset by a distance 2Δ . (b) The Gouy phase shifts associated with the two beams. (c) Difference of the Gouy phases.

2.1 Polarization conversion

To demonstrate the polarization conversion that occurs near the beam foci, consider first points on the beam axis, for which

$$I(0, z) = [1 + (z/z_o)^2]^{-1}, \quad \phi(0, z) = -kz + \eta(z). \quad (8)$$

The intensity has a Lorentzian distribution of FWHM width $2z_o$ and a peak value of unity at $z = 0$. The phase $\eta(z) = \arctan(z/z_o)$ is the axial phase anomaly known as the Gouy phase shift [17, 18]. It increases monotonically from $-\pi/2$ at $z = -\infty$ to $\pi/2$ at $z = \infty$, with zero value at $z = 0$. For a combination of two such beams with an axial offset 2Δ , as in Eq. (6), the phase difference between the two beams, $\eta(z-\Delta) - \eta(z+\Delta) + 2k\Delta - \xi$, varies with z , and so does the state of polarization. As illustrated in Fig. 1, the difference of the Gouy phases is approximately zero, except near the beam foci, where it can reach a maximum value of π at $z = 0$. This may be exploited to effect a conversion of the polarization state that is confined to the focal region. For example, if the constant phase $2k\Delta - \xi = \pi/2$, then the combined beam is in the RCP state at axial points far from the focal region, and in the LCP state at $z = 0$. This conversion from RCP to LCP and back to RCP on axis as the beam travels through the focal region is attributed to the Gouy effect. We will hereafter call the RCP and LCP components the “majority” and “minority” polarizations, respectively. We will show that for certain values of the ratio Δ/z_o , called the offset parameter, the focal volume of the minority polarization may be smaller than that of the constituent Gaussian beam, thus potentially achieving axial superresolution, lateral superresolution, or both.

2.2 Spatial distributions

The spatial distributions of the circularly-polarized components may be readily determined by using Eqs. (4)-(7) and when $2k\Delta - \xi = \pi/2$ the intensities of the RCP and LCP components become

$$I_{R,L}(\rho, z) = I_o(\rho, z) \pm I_1(\rho, z) \cos[\zeta(\rho, z)], \quad (9)$$

where

$$I_o(\rho, z) = \frac{1}{2}[I(\rho, z - \Delta) + I(\rho, z + \Delta)], \quad (10)$$

$$I_1(\rho, z) = [I(\rho, z - \Delta)I(\rho, z + \Delta)]^{1/2}, \quad (11)$$

$$\zeta(\rho, z) = \eta(z - \Delta) - \eta(z + \Delta) - k\rho^2/2R_1(z), \quad (12)$$

$$1/R_1(z) = 1/R(z - \Delta) - 1/R(z + \Delta). \quad (13)$$

In any transverse plane $z \neq 0$, the intensities of the circularly-polarized components are modulated by radial patterns in the form of chirped rings similar to the zones of Fresnel plates. These annular patterns result from interference between Gaussian components with different wavefront curvatures. As we shall subsequently see, such patterns can result in radial confinement in the focal region ($z = 0$). Annular apertures are known to correspond to tighter focus [19, 20, 21, 22].

2.3 Axial superresolution

It can be shown that the axial intensity distribution of the LCP component $I_L(0, z)$, as given by Eqs. (9)-(13) at $\rho = 0$, is a bell-shaped function with a single peak at $z = 0$, if the offset $\Delta < z_o$. A greater offset corresponds to a double-peaked axial distribution, which is not surprising since it is known that the peak intensity of a spherical wave transmitted through an annular aperture is displaced from the geometrical focus, a phenomenon known as the focal shift [23]. The FWHM of $I_L(0, z)$ is given by

$$z_{FWHM}^{(L)} = 2z_o\{[2(1+r^4)]^{1/2} - (1-r^2)\}^{1/2}, \quad (14)$$

where $r = \Delta/z_o$ is the offset parameter. For $|r| < 0.67$, $z_{FWHM}^{(L)} < 2z_o$, i.e., the LCP beam has an axial width smaller than that of the conventional Gaussian beam. This axial superresolution effect increases as Δ is reduced, but the peak intensity

$$I_L(0, 0) = 2r^2/[1+r^2]^2 \quad (15)$$

is also reduced, eventually vanishing as $\Delta \rightarrow 0$. As an example, if $r = \Delta/z_o = 0.25$, the normalized axial width $z_{FWHM}^{(L)}/2z_o = 0.69$ and the intensity is 0.11, i.e., the axial width is compressed by a factor of approximately 1.45 and the intensity is reduced to 11% of its value for the constituent Gaussian beam. The axial distributions of the compressed LCP beam and the constituent Gaussian beams are compared in Fig. 2(a), and the dependence of the axial width and peak intensity on the offset parameter is shown in Fig. 3.

2.4 Transverse superresolution

One measure of transverse superresolution is the reduction in the radial width of the intensity distribution in the $z = 0$ plane. In this plane, $I_o(\rho, 0) = I_1(\rho, 0) = I(\rho, \Delta)$ so that Eq. (9) becomes

$$\begin{aligned} I_L(\rho, 0) &= 2I(\rho, \Delta) \sin^2[\zeta(\rho, z)/2], \\ &= \frac{2}{1+r^2} \exp\left(-\frac{2}{1+r^2} \frac{\rho^2}{W_o^2}\right) \sin^2\left[\arctan(r) - \frac{r}{1+r^2} \frac{\rho^2}{W_o^2}\right] \end{aligned} \quad (16)$$

This is a Gaussian function of ρ modulated by a \sin^2 function of ρ^2 . When plotted as a function of the ratio ρ/W_o , the width is completely determined by the offset parameter $r = \Delta/z_o$. For example, when the offset parameter $r = 0.25$, the FWHM radial width is 0.84, as compared to

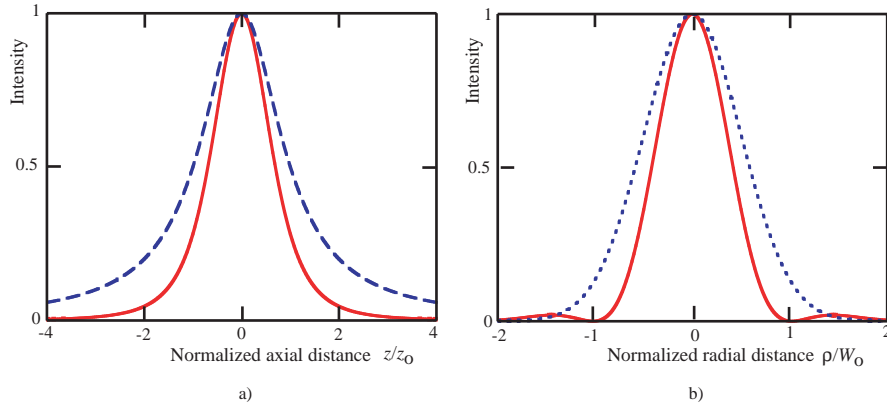


Fig. 2. (a) Axial distributions of the LCP component (solid curve) and the constituent Gaussian linearly polarized beam (dashed). (b) Radial distributions of the LCP component (solid curve) and the constituent Gaussian linearly polarized beam (dashed).

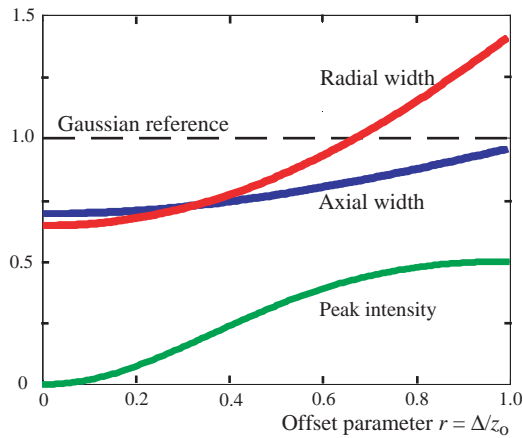


Fig. 3. Dependence of the axial and radial widths (FWHM) and the peak intensity of the LCP (minority) component on the offset parameter $r = \Delta/z_0$. All values are normalized to the corresponding values for the constituent Gaussian beam.

1.18 for the constituent Gaussian beam. This is an improvement by a factor of 1.4. As illustrated in Fig. 2(b), this compression is accompanied by a small side lobe. Reduction of the offset parameter leads to further improvement of the lateral resolution, at the expense of a reduction in peak intensity, as illustrated in Fig. 3.

The distribution of the LCP beam at off-axis or off-focal-plane points may be determined by use of Eqs. (4)-(7). Figure 4 has a plot of the intensity in a meridional plane ($x = 0$) for the LCP beam and a constituent Gaussian beam whose center is at $(x, z) = (0, 0)$. The offset parameter $r = 0.25$. Clearly, the LCP beam has a focal spot smaller than that of the Gaussian beam. The distribution of the LCP beam in a transverse plane at a distance $z = 5z_0$ from the center is also shown in Fig. 4, demonstrating the annular distribution of the LCP beam.

2.5 Power exchange

The change of the state of polarization and the spatial redistribution of optical intensity, which accompanies wave propagation, raise the question of power exchange between the polarization modes. It can be shown, however, that if the medium and the optical components are linear, isotropic, and lossless, then the total power (intensity integrated over the transverse plane) in each of the two orthogonally polarized beams is fixed, i.e., invariant to the axial distance z .

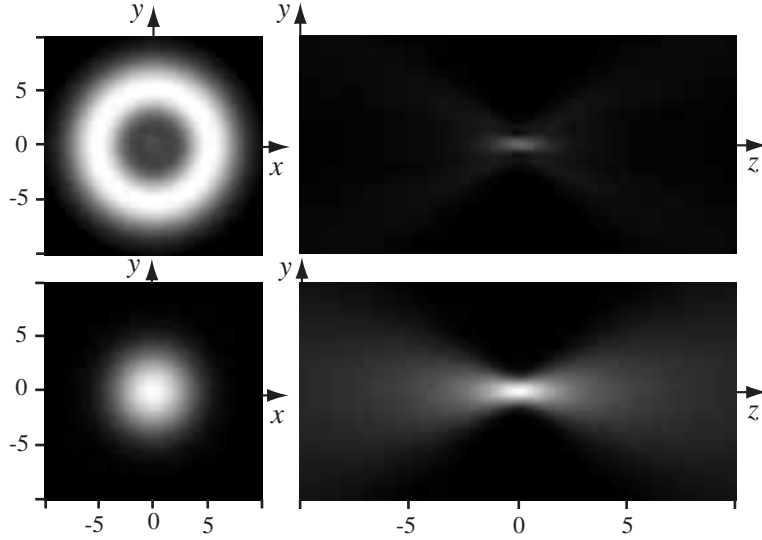


Fig. 4. Intensity distribution of the LCP beam (top) and a reference linearly polarized Gaussian beam (bottom). The distributions in the meridional plane $x = 0$ (right) and the transverse plane $z/z_0 = -5$ (left) are shown. The axial position z is in units of z_0 and the transverse dimensions are in units of W_0 . The offset ratio $r = \Delta/z_0 = 0.25$. In each figure, the intensity is normalized such that the maximum value is unity.

Consider the expansion in Eq. (2) in terms of RCP and LCP beams. Each of these polarization components propagates linearly and independently, and the propagation may be described by a polarization-independent Green's function $G^{(z)}(x, y; x', y')$, which relates the distribution in a transverse plane at the position z to that in the $z = 0$ plane,

$$f_{\mathbf{R},\mathbf{L}}(x, y, z) = \iint dx' dy' G^{(z)}(x, y; x', y') f_{\mathbf{R},\mathbf{L}}(x', y', 0). \quad (17)$$

Since the medium is lossless, the Green's function must obey the unitarity relation

$$\iint dx dy G^{(z)}(x, y; x', y') G^{(z)*}(x, y; x'', y'') = \delta(x' - x''; y' - y''). \quad (18)$$

Using Eqs. (17) and (18), it can be shown by direct substitution that in any plane perpendicular to the axis of propagation, the total power in each of the polarization components is invariant to z , e.g.,

$$P_{\mathbf{R}}(z) = \iint dx dy |f_{\mathbf{R}}(x, y, z)|^2 = \iint dx dy |f_{\mathbf{R}}(x, y, 0)|^2 = P_{\mathbf{R}}(0). \quad (19)$$

Similarly, $P_{\mathbf{L}}(z) = P_{\mathbf{L}}(0)$. We therefore conclude that in any plane perpendicular to the axis of propagation, the ratio of the RCP and LCP powers remains constant. A similar result is applicable to the \mathbf{x} and \mathbf{y} polarizations, or any other set of orthogonal polarizations.

3. Focusing of superposed Gaussian beams by a lens

A possible implementation of polarization-assisted superresolution is based on focusing two orthogonally polarized Gaussian beams of different curvatures by use of an objective lens, as illustrated in Fig. 5. At the entrance of the lens, the two beams have the same width, but one beam is completely collimated and the other is slightly divergent. For instance, we assume here that the beams are linearly polarized in the \mathbf{x} and \mathbf{y} directions, although the same argument applies to any other pair of orthogonal polarizations. The phase difference between the two

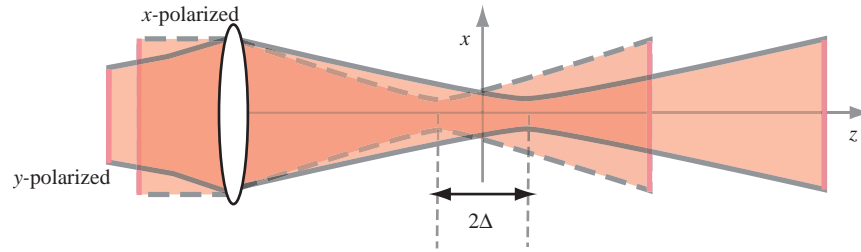


Fig. 5. Proposed scheme for creating polarization-assisted superresolution. Two Gaussian beams of the same width and with a slight difference in curvature are focused by a lens. The x - and y -polarized components have a 90° phase shift at the beam axis. The left-circularly polarized component (minority) is highly confined in the focal region.

beams is selected such that the total field at the lens plane on the beam axis is in the RCP state, the majority polarization.

Because of the difference between the divergences of the two beams, the x -polarized beam focuses slightly closer to the lens than does the y -polarized beam, so that the centers of the focused beams are axially offset, but in this geometry the Gaussian beams do not have the same parameters. As mentioned earlier, as a result of the Gouy phase shifts encountered near the foci of the beams, a phase shift is introduced between the x - and y - polarized beams in the vicinity of the focal spot. In a small region of space between the foci of the two beams where that phase shift is near π , the polarization at the on-axis points is approximately converted to LCP (minority polarization).

As an example, we have examined a system operating at a $1\text{-}\mu\text{m}$ wavelength. The beams have an initial width $W = 1\text{ mm}$ in the lens plane and the lens has a 4-mm focal length. If the uncollimated beam has a radius of curvature $R = 1.572\text{ mm}$ before it enters the lens, then the focused beams will have waists $W_o = 1.2732\text{ }\mu\text{m}$ and $1.2740\text{ }\mu\text{m}$ and Rayleigh ranges $z_o = 5.093\text{ }\mu\text{m}$ and $5.099\text{ }\mu\text{m}$, so that the two beams have approximately equal parameters. Their centers are offset by a distance $2\Delta = 2.505\text{ }\mu\text{m}$ corresponding to an offset ratio $r = \Delta/z_o \approx 0.25$. We have computed the axial and radial distributions of the intensity of the majority (RCP) and minority (LCP) polarization components at points within the focal volume for this system. The intensity distribution of the minority polarization in a meridional plane in the focal region is shown in Fig. 6. Contours of constant intensity (isophotes) at fixed fractions of the peak value are also shown. For comparison, the same plots are also shown for a reference Gaussian beam focused at a point midway between the foci of the input x - and y -polarized beams and having their same width in the lens plane. Based on the 3-dB contours, we conclude that the distribution of the minority polarization is tighter than that of the reference beam by factors of 1.45 and 1.4 in the axial and radial directions, respectively. The total power of the minority polarization is approximately 11% of the total input power. The PAS technique described in this section may also be implemented by transmitting a single circularly polarized Gaussian beam through a birefringent lens, which introduces different wavefront curvatures into the x - and y -polarized components. Alternatively, these two components may be separated with a polarizing beam splitter and recombined with another beam splitter after traveling slightly different distances, as in a Mach-Zehnder interferometer. Interferometric methods have been used in creating desired spatial distributions in the focal region [14] and in the generation of standing-wave excitation for enhanced-resolution fluorescence microscopy [24]. Yet another possible implementation is based on the use of a birefringent slab, or etalon, inside a laser cavity arranged such that x - and y -polarized Gaussian modes are generated with offset foci.

Since the Gouy effect is not limited to Gaussian beams, other beams are expected to yield similar PAS under similar conditions. An example is the beam generated by focusing a plane wave with a perfect lens of finite circular aperture. This beam has a Bessel-type radial in-

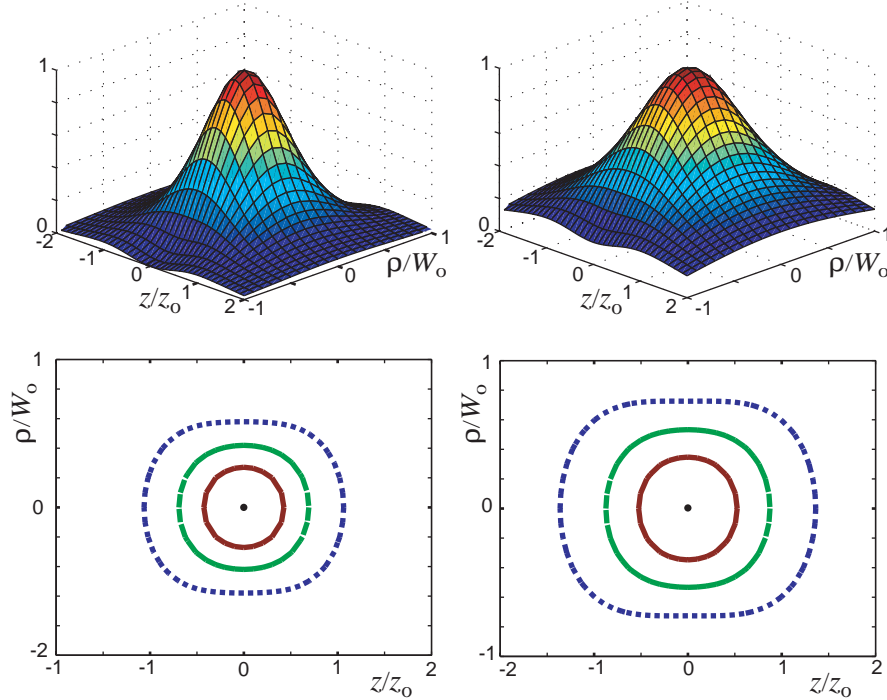


Fig. 6. Intensity distributions (above) and contours of constant intensity (below) for the minority component (left) and the reference Gaussian beam (right). The contours are at fractions of the peak intensity of 2/3 (solid red line), 1/2 (dashed green line), and 1/3 (dotted blue line).

tensity distribution and a sinc^2 axial intensity distribution [25]. The Gouy phase decreases linearly from $\pi/2$ to $-3\pi/2$ as z/z_0 increases from -4π to 4π , and outside this range it changes periodically following a sawtooth function with period $4\pi z_0$ and amplitude π [25]. Here, $z_0 = (\lambda/2\pi)(f^2/a^2)$, where a is the radius of the aperture and f is the lens focal length (for a Gaussian beam of width W at the lens, z_0 has the same expression with a replaced by $W/\sqrt{2}$). Two such beams whose centers are offset by a distance $\Delta = 4\pi z_0$, equal to the period, result in a Gouy phase difference of π at axial points between $z = 0$ and $z = 4\pi z_0$, and zero elsewhere. This rectangular profile corresponds to the bell-shaped profile in Fig. 1c for the Gaussian beam. The minority polarization component is therefore expected to be confined between $z = 0$ and $z = 4\pi z_0$ on axis. Also, since the transverse distribution of the minority polarization in the plane of the lens has an annular pattern, transverse superresolution in the focal plane is also expected, but with side lobes larger than in the Gaussian beam case.

4. Conclusion

We have shown that a combination of **x**- and **y**-polarized Gaussian beams, with a 90° phase shift and slightly offset foci, corresponds to right-circularly polarized (majority) and left-circularly polarized (minority) beams with non-Gaussian spatial distributions. For an offset distance of the order of half the Rayleigh range, the minority beam has a smaller focal volume than the constituent Gaussian beam. The origin of this polarization-assisted radial and axial superconfinement lies at the annular distribution of the minority beam, which results from the interference of two wavefronts with different curvature. It may alternatively be attributed to the differential axial phase anomalies, or Gouy phases, of the constituent linearly-polarized Gaussian beams.

Although the polarization state is converted from RCP at the input plane into LCP at the focal region (at points on the beam axis), it is important to note that the total power carried by

each mode is invariant to the axial position. The two modes propagate independently, and the fixed power in each mode is redistributed in the lateral plane as it travels. Polarization-assisted superresolution is achieved by mixing two linearly polarized Gaussian beams, which are convenient to generate, thus creating a non-Gaussian circularly polarized wavefront that is naturally focused into a tighter focal spot, independently of the other orthogonal mode. Should such non-Gaussian wavefront be created by some other mechanism, the wavefront would naturally be focused to the tighter spot.

This superconfinement can be taken advantage of in laser scanning fluorescence imaging and lithography. The effect can be enhanced further through two-photon or multi-photon processes [11], and any side lobes that may appear in the radial profile can be suppressed in threshold dependent material systems or in confocal imaging systems.

Acknowledgments

This work was supported by the National Science Foundation (Grant No. ECS-0088438); the Center for Subsurface Sensing and Imaging Systems (CenSSIS), an NSF Engineering Research Center; and the David and Lucile Packard Foundation. JTF is a Research Corporation Cottrell Scholar and a Camille Dreyfus Teacher Scholar. The assistance of Jason Stewart is acknowledged.